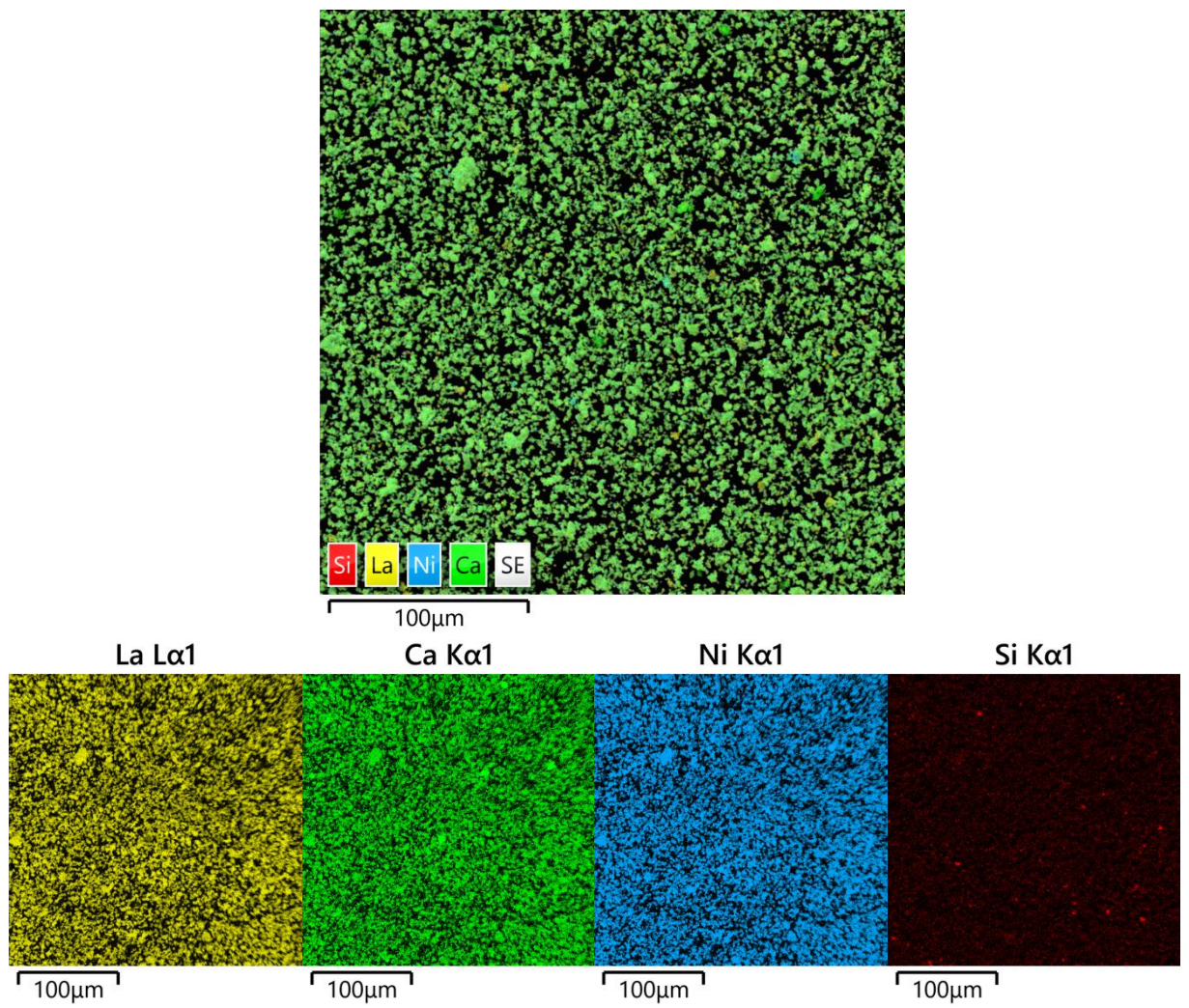


**Table S1.** Impurity content (according to the ICP-OES data) and specific surface area (according to the BET analysis data) of the  $\text{La}_{1.7}\text{Ca}_{0.3}\text{Ni}_{1-y}\text{Cu}_y\text{O}_{4+\delta}$  powders after the two-stage synthesis with intermediate and final milling.

	Impurity content, wt. %		$S_{\text{BET}}$ , $\text{m}^2 \cdot \text{g}^{-1}$
	Si	Fe	
0.0	0.41	0.38	1.16(2)
0.2	0.39	0.33	0.94(1)
0.4	0.42	0.41	0.97(2)

**Table S2.** Impurity content in the  $\text{La}_{1.7}\text{Ca}_{0.3}\text{Ni}_{1-y}\text{Cu}_y\text{O}_{4+\delta}$  powders determined by SEM/EDS analysis.

y	Fraction of impurities, wt. %			Fraction of impurities, at. %	
	Si	Fe		Si	Fe
0	0.41	0.53		0.63	0.41
0.2	0.7	0.36		1.18	0.3
0.4	0.74	0.36		1.17	0.29



**Figure S1.** SEM/EDS elemental distribution maps of the  $\text{La}_{1.7}\text{Ca}_{0.3}\text{NiO}_{4+\delta}$  powder

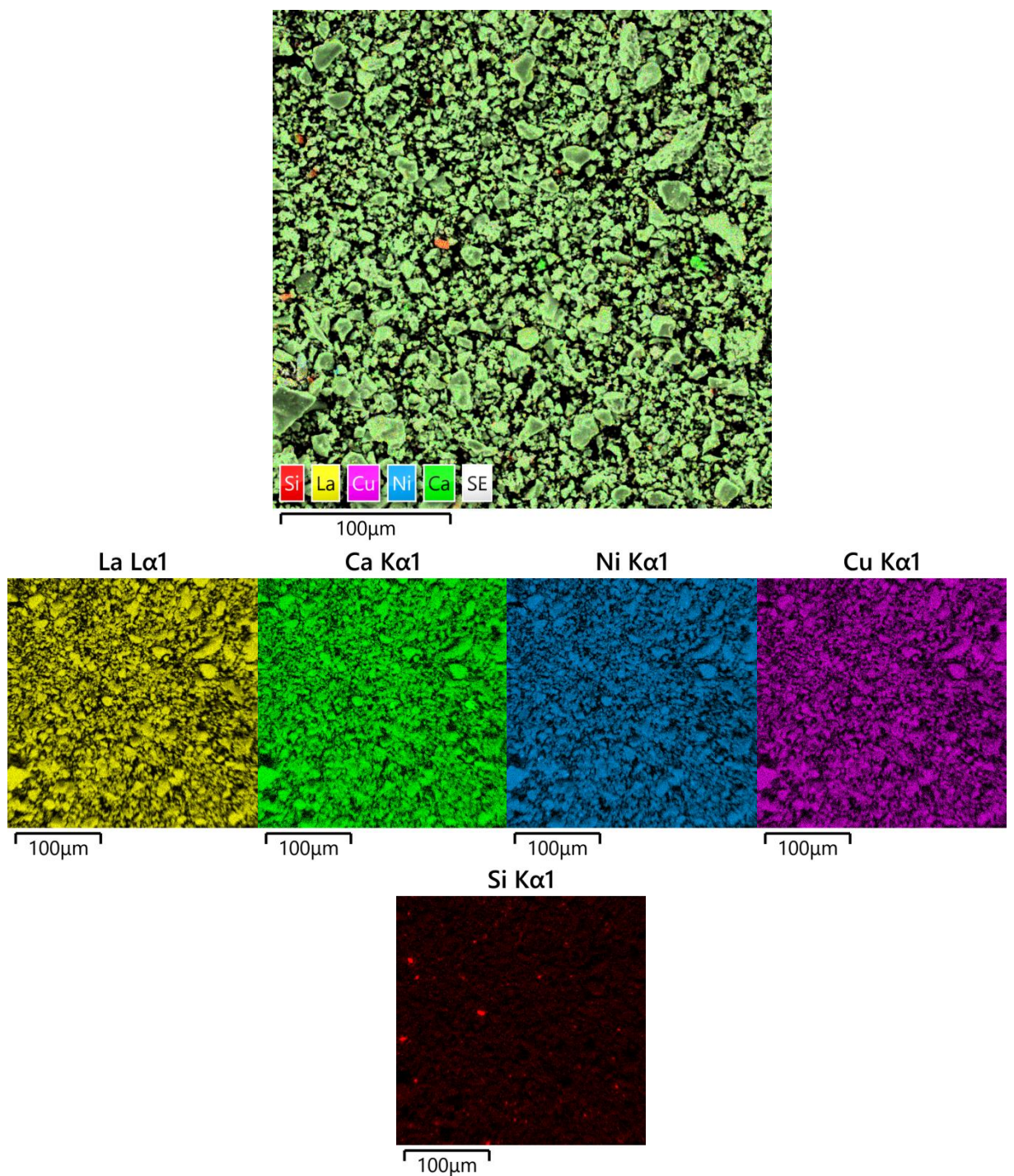


**Figure S2.** SEM/EDS elemental distribution maps of the  $\text{La}_{1.7}\text{Ca}_{0.3}\text{Ni}_{0.8}\text{Cu}_{0.2}\text{O}_{4+\delta}$  powder

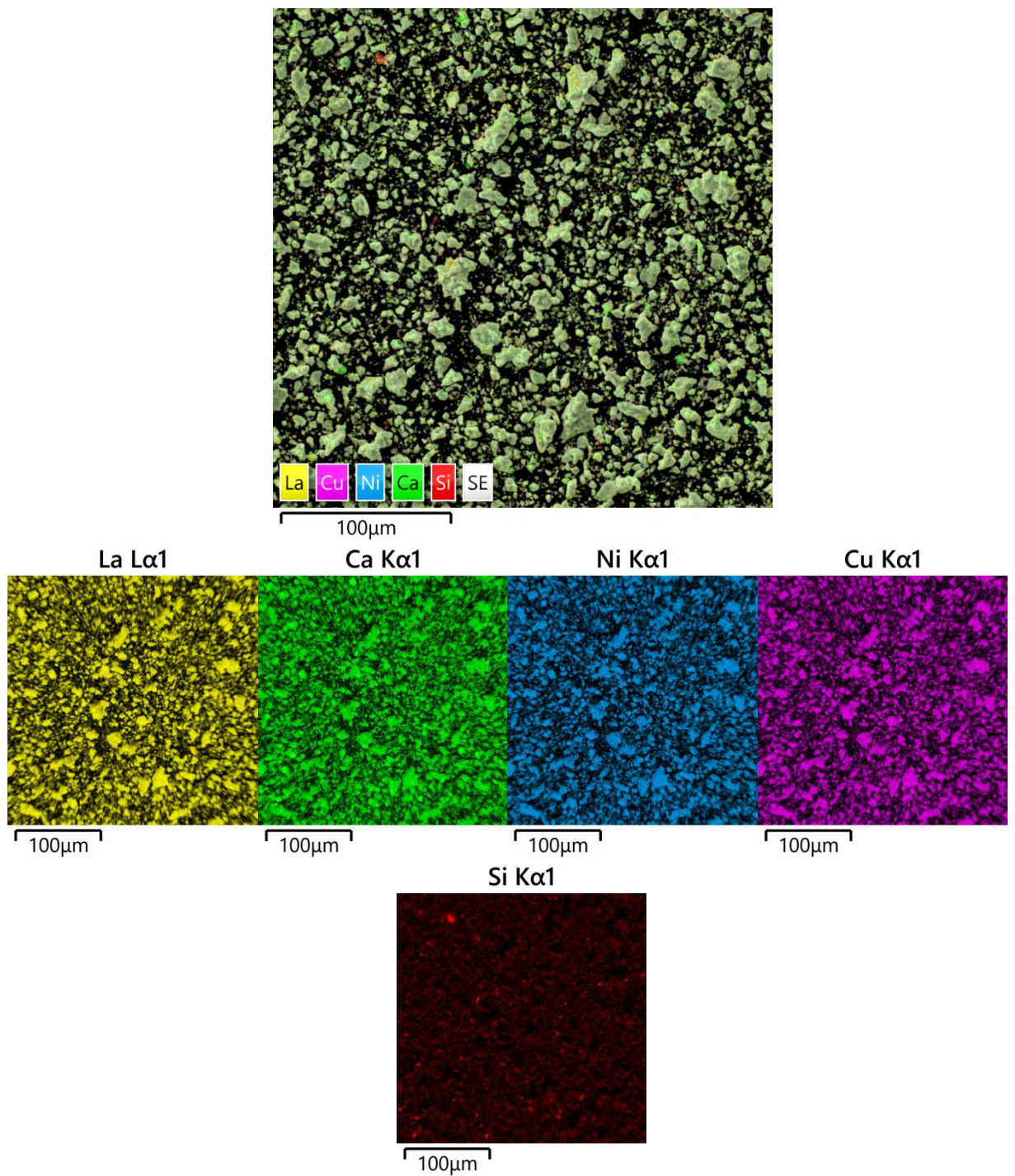


**Figure S3.** SEM/EDS elemental distribution maps of the  $\text{La}_{1.7}\text{Ca}_{0.3}\text{Ni}_{0.6}\text{Cu}_{0.4}\text{O}_{4+\delta}$  powder

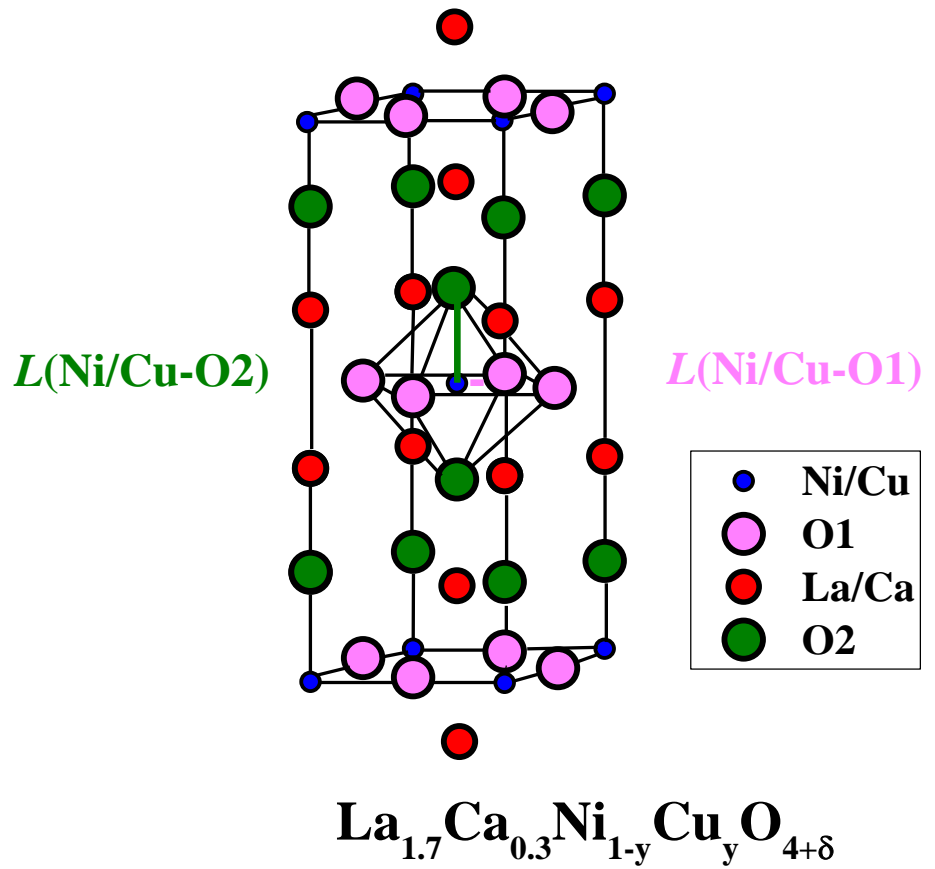


**Figure S4.** Crystal structure of  $\text{La}_{1.7}\text{Ca}_{0.3}\text{Ni}_{1-y}\text{Cu}_y\text{O}_{4+\delta}$ .

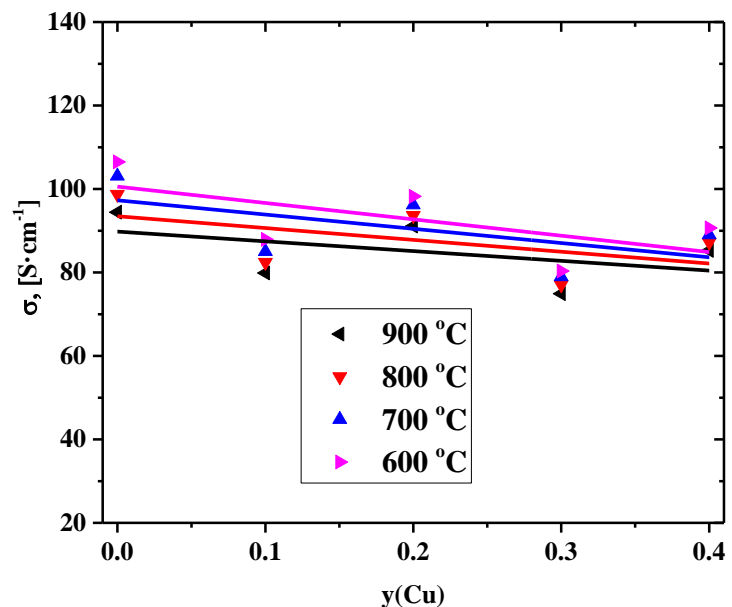


**Figure S5.** Concentration dependencies of the total conductivity of the  $\text{La}_{1.7}\text{Ca}_{0.3}\text{Ni}_{1-y}\text{Cu}_y\text{O}_{4+\delta}$  compact samples collected in air.

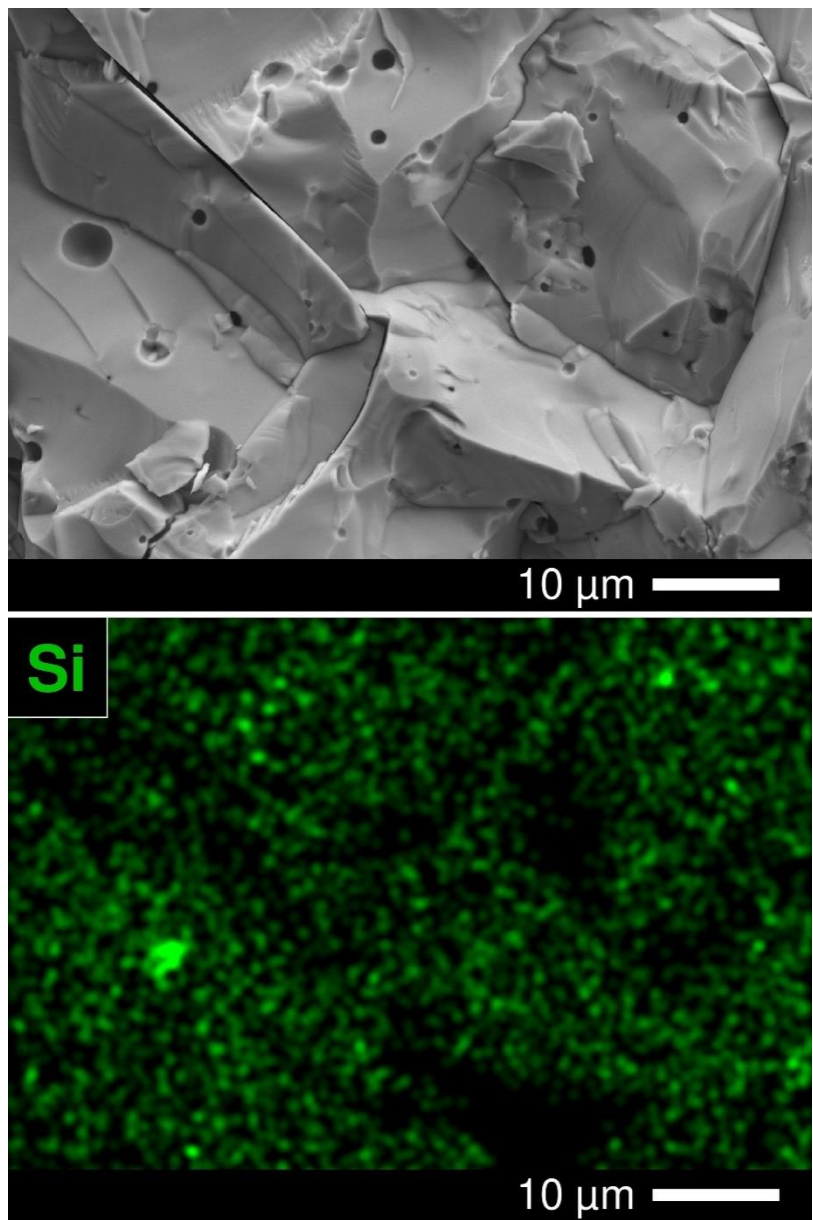


**Figure S6.** SEM/EDS: fractured surface of  $\text{La}_{1.7}\text{Ca}_{0.3}\text{Ni}_{0.8}\text{Cu}_{0.2}\text{O}_{4+\delta}$  ceramics sintered at 1380 °C.

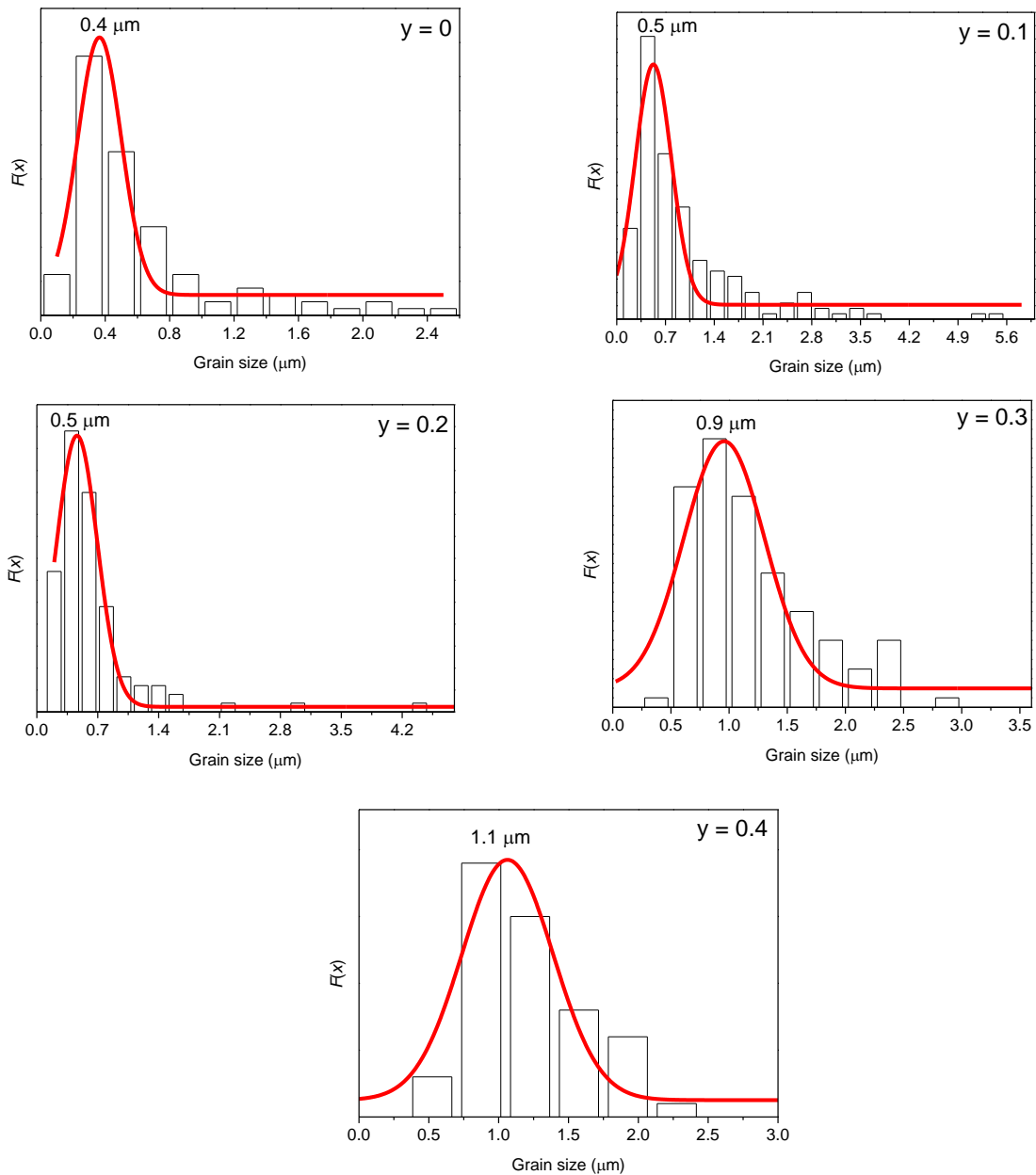


**Figure S7.** Particle size distribution in the  $\text{La}_{1.7}\text{Ca}_{0.3}\text{Ni}_{1-y}\text{Cu}_y\text{O}_{4+\delta}$  electrodes based on the SEM data.

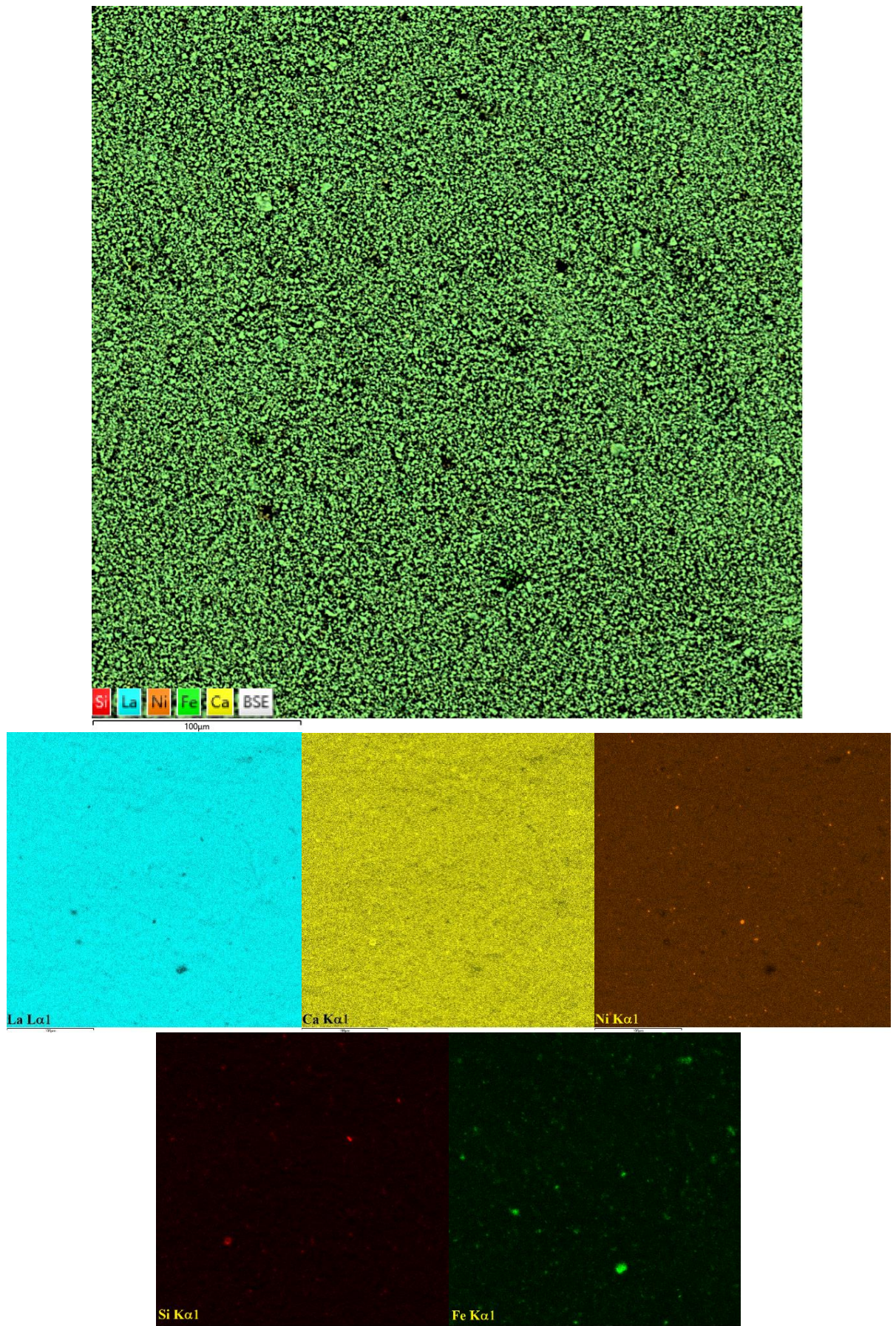


**Figure S8.** SEM/EDS elemental distribution maps of the  $\text{La}_{1.7}\text{Ca}_{0.3}\text{NiO}_{4+\delta}$  electrode surface ( $T_S = 1000^\circ\text{C}$ ).

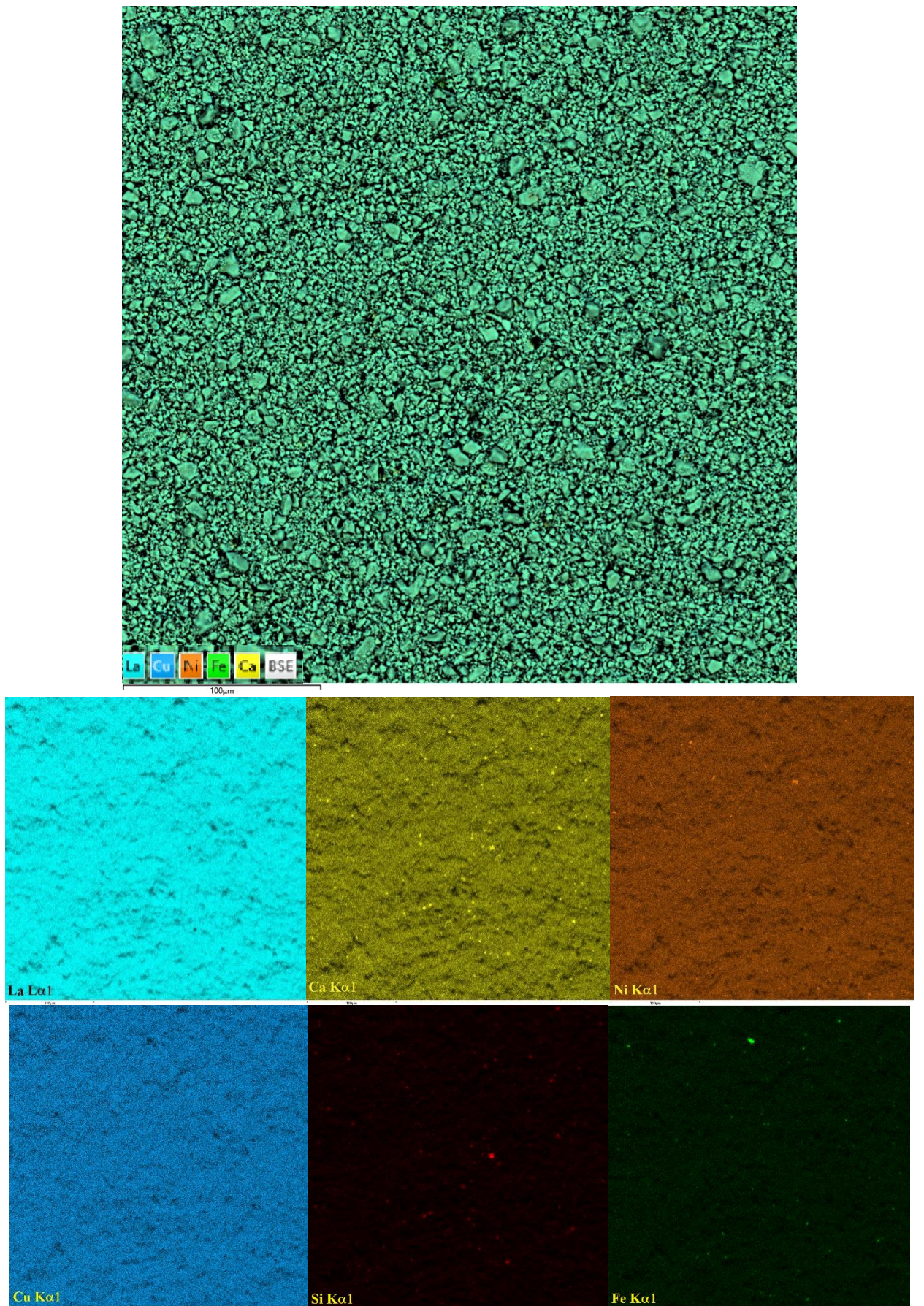


**Figure S9.** SEM/EDS elemental distribution maps of the  $\text{La}_{1.7}\text{Ca}_{0.3}\text{Ni}_{0.8}\text{Cu}_{0.2}\text{O}_{4+\delta}$  electrode surface ( $T_s = 1000^\circ\text{C}$ ).

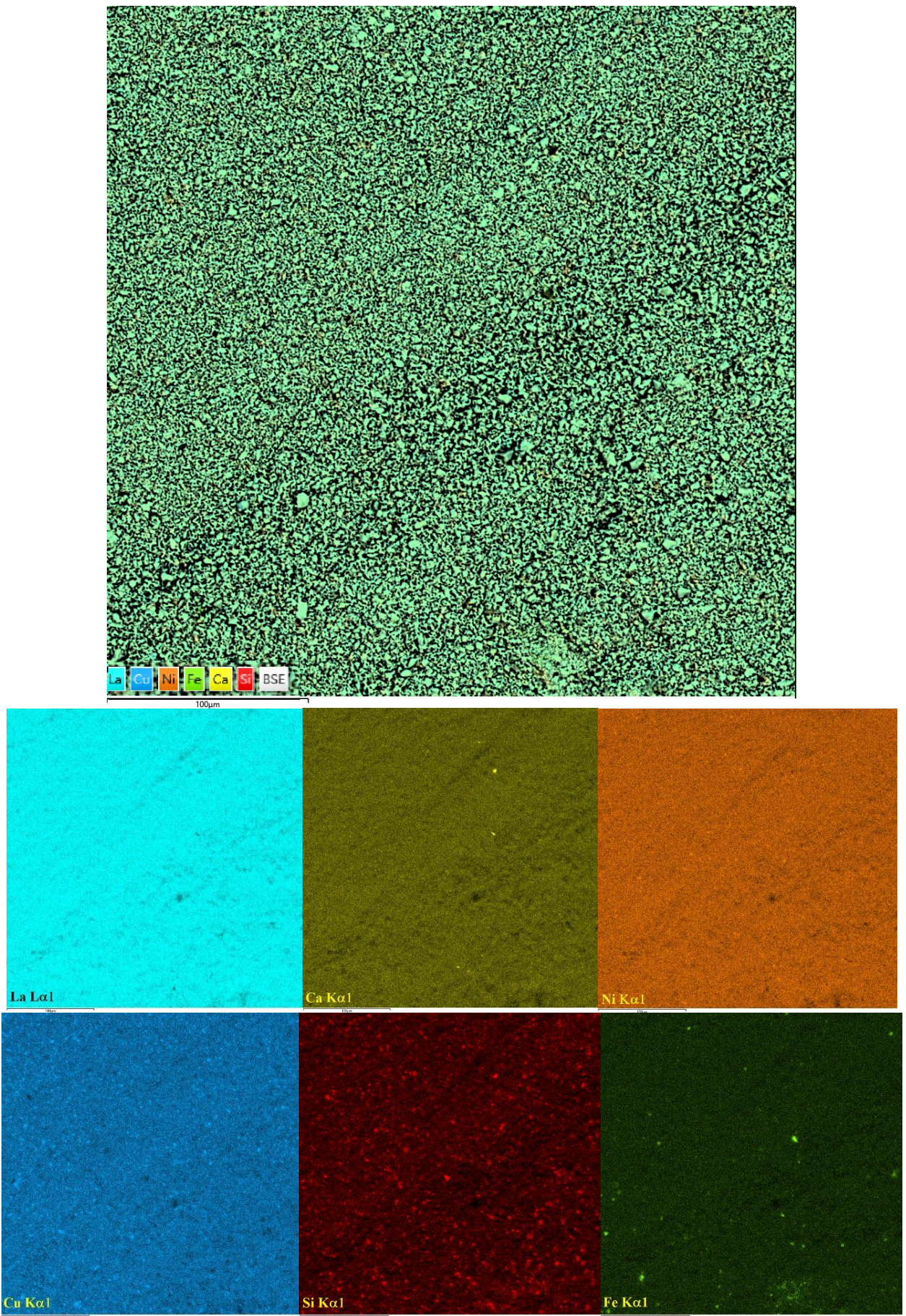


**Figure S10.** SEM/EDS elemental distribution maps of the  $\text{La}_{1.7}\text{Ca}_{0.3}\text{Ni}_{0.6}\text{Cu}_{0.4}\text{O}_{4+\delta}$  electrode surface ( $T_s = 1000^\circ\text{C}$ ).

**Table S3.** Chemical composition of  $\text{La}_{1.7}\text{Ca}_{0.3}\text{Ni}_{1-y}\text{Cu}_y\text{O}_{4+\delta}$  electrodes determined by SEM/EDS analysis of the electrode surface.

y	Fractions of metal cations, at. %							La:Ca:Ni:Cu
	La	Ca	Ni	Cu	Si	Fe	Pt	
0	54.30	9.39	32.07	-	2.00	1.11	1.13	1.69:0.29:1.00:0
0.2	54.00	9.54	26.09	6.26	2.45	0.80	0.87	1.66:0.29:0.80:0.19
0.4	53.55	9.33	19.21	12.68	3.46	1.03	0.75	1.67:0.29:0.60:0.40

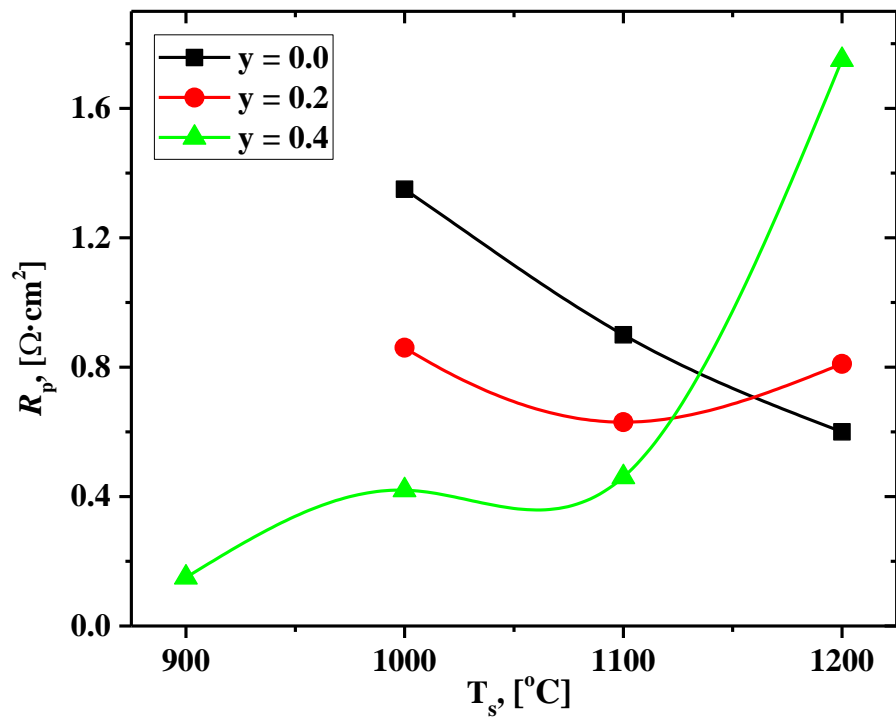


**Figure S11.** Influence of electrode sintering temperature on the polarization resistance of  $\text{La}_{1.7}\text{Ca}_{0.3}\text{Ni}_{1-y}\text{Cu}_y\text{O}_{4+\delta}$  electrodes in contact with SDC solid electrolyte.